Research on Variable Frequency Transformer: A Smart Power Transmission Technology

MOHD MOHSIN KHAN[ID][1]**, IMDADULLAH**[ID][2]**, (Senior Member, IEEE), JAMEL NEBHEN**[ID][3]**, AND HAFIZUR RAHMAN**[ID][1]

[1]Department of Electrical Engineering, Zakir Husain College of Engineering and Technology, Aligarh Muslim University, Aligarh 202002, India
[2]Electrical Engineering Section, University Polytechnic, Faculty of Engineering and Technology, Aligarh Muslim University, Aligarh 202002, India
[3]Prince Sattam bin Abdulaziz University, College of Computer Engineering and Sciences, Alkharj 11942, Saudi Arabia

Corresponding authors: Mohd Mohsin Khan (mohdmohsinkhanee@gmail.com) and Imdadullah (imdadamu@gmail.com)

ABSTRACT The electric power systems are interconnected for the economical and reliable operation of power supply systems. An interconnection of power systems can be implemented through AC and DC links. A variable frequency transformer (VFT) has emerged as an alternative for asynchronous interconnection, like back-to-back HVDC links. Unlike back-to-back HVDC links, VFT requires reduced reactive power, offers quicker incipient transient recovery, and has coherent damping ability. Various control strategies have been proposed in the literature to achieve the controllable and reliable operation of VFT. The VFT can be scalable for high power exchange by implementing the VFT Park model. The VFT is essentially a doubly-fed induction machine (DFIM) based system that needs slip rings and brushes in the rotor circuit. Hence, brushless doubly-fed induction machine (BDFIM) based VFT systems and their various topologies are proposed in the literature. In this paper, a comprehensive review is carried out, which includes: power system networks interconnection philosophy, power flow controllers used in the interconnected networks, FACTS controllers, and HVDC link with their technical merits and limitations. A comparison of VFT with its counter technology back-to-back HVDC link is also elaborated, which suggests VFT a better option for asynchronous grid interconnection. Moreover, a thorough literature review is done concerning VFT configuration, controls, and scaling with research papers and patents. Furthermore, detailed mathematical modeling of the VFT system is also carried out along with the numerical simulations under both steady-state and various fault conditions using PSCAD/EMTDC software.

INDEX TERMS Asynchronous interconnection, power flow controllers, FACTS, HVDC, variable frequency transformer (VFT), brushless doubly-fed induction machine (BDFIM), doubly-fed induction machine (DFIM).

I. INTRODUCTION

The fast-growing population requires industrialization at a substantial level to cope with their needs, particularly for developing and underdeveloped nations. The fast industrial development would lead to the rapid and consistent growth in energy demand [1]. In addition, a deficit of fossil fuels would hurdle energy development, and many nations are facing this challenge and hence looking forward to it. One possible solution is to expand their renewable energy based electricity generation. However, the successful implementation of various renewable energy resources is not relatively

The associate editor coordinating the review of this manuscript and approving it for publication was Jahangir Hossain[ID].

easy because of their uncertain nature, and the stability of the power grid is not assured [2]–[4].

A. MOTIVATION AND INCITEMENT

To meet enormous energy demand, most national, regional, urban, and rural grids opted for grid interconnection [5]. The resulting grid interconnection offers greater reliability, thereby offering reduced electricity generation cost and improves the power supply services [6]. In addition, the interconnection of power networks avoids generating reserve requirements in each system. Thus, interconnection abates investment in energy production or somewhat halts the need to add new capacity soon. Furthermore, the interconnection of power system networks leads to the ease of the electricity

market. It enables the commercialization of power through multiple provinces and nations. Most power system networks in the world today operate at either 50 Hz or 60 Hz frequencies. The integration of nearby power networks is a dynamic approach to the global energy system today, and further research in this field is of quite an interest globally. There is a development of multiple microgrids, integration of multiple renewables to the utility grids, and the interconnection of various national, regional and local power grids [7]–[10]. Due to the above facts, many researchers and power engineers are looking forward to various grid interconnection technologies and different power flow controllers.

B. LITERATURE REVIEW

To interconnect two power systems, a reliable and cost-effective interconnector (link) is required. Two power systems may be interconnected via synchronous interconnection and asynchronous interconnection. The synchronous interconnection allows the interconnection of power grids operating at the same frequency through an AC link. This arrangement offers simplicity as well as economic feasibility [11]. However, this method imposes complexity in the operation of the power system. Moreover, it also imposes serious stability limitations under severe fault conditions [12].

The control of power transfer through these connection lines is regulated by different power flow controlling devices such as phase-shifting transformer (PST) [13], [14], sen transformer (ST) [15], [16], rotary power flow controller (RPFC) [17], [18], and FACTS controller [19]. In the case of PST, the power flow can be assessed by controlling the line voltage vector. However, control of power transfer is accompanied in steps by changing the tapings of the transformer, which ultimately results in sluggish control of power. Independent control of real and reactive power flow can be attained by using Sen Transformer (ST) [20]. However, ST has limitations of output error and sluggish response [15], [21]. The RPFC claims better results than PST but requires an isolated drive system for rotation of rotor shaft [22]. A comparative study of various power flow controllers used for controlling the power flow in synchronous interconnected power systems is presented in Table 1.

The FACTS controller is emerging from the roots of power electronics to control one or more power transmission parameters. There are various FACTS controllers which have been evolved for the control of power transfer through AC link. The conventional FACTS controller is static var compensator (SVC) which is a variable impedance type. The SVC is usually placed in a shunt with the power network. Moreover, the thyristor switched series reactor (TSSR), thyristor-controlled series reactor (TCSR), thyristor-controlled series capacitor (TCSC) are series FACTS controllers. However, drawbacks related to these controllers are the injection of current harmonics, and their sluggish response [33]. Table 2 summarizes various FACTS controllers used for controlling the power flow in the interconnected power system networks.

The other method of the interconnection of two power systems operating at the same or different frequencies is asynchronous interconnection. A high voltage direct current (HVDC) system is a common technique to implement asynchronous interconnection. The HVDC system is economical for large distances and a huge amount of power transfer. However, the high cost of converters, demands of reactive power, production of harmonics, and the problems of circuit breaking restricts its applications [45]–[47]. Moreover, HVDC link also has operating problem where low AC power is linked on any of the two sides [48]. A summary of various HVDC topologies used for asynchronous interconnections are presented in Table 3.

An asynchronous interconnection may also be made by a virtual synchronous machine (VSM) to integrate distributed generators (DGs) into the utility grid. The concept of VSM has evolved to provide aspects of controllability and stability of a conventional synchronous machine in the control of power electronic converters [62]. The problems associated with the installation of VSM include generating oscillations of reduced frequency in the power systems, which is a result of interaction between the synchronous generators [63].

Alternatively, asynchronous interconnection can also be made by the variable frequency transformer (VFT). Over the past decade, the VFT has proven itself to be an effective means for asynchronous interconnection, and a perfect contender of PST in synchronous interconnection [64], [65]. The VFT was initially introduced by General Electric (GE) in the US in the 1990s and successfully used on the power grid in the early 21st century. The world's maiden VFT was developed at Hydro-Quebec's Langlois substation in October 2003, where it used to transport 100 MW of electric power between the power grids of Quebec, Canada, and New York, US [66]–[68]. A negotiation was signed in 2001 with corporations for installing a 100 MW VFT at Langlois substation. Initially, many simulator tests were performed to verify the adaptableness nature of VFT, and the VFT was then tested in the physical environment in 2003. The VFT was first used in operation as a phase-shifter in parallel with the local network in April 2004 for eight months. Due to the continuous satisfying operation during this period, finally, the industrial operation commenced in April 2005. The successful operation of the maiden VFT gained a significant attraction of researchers, and its application scope began to extend. Consequently, the world's next VFT was financed by American Electric Power (AEP) and produced by GE. This VFT was established at Laredo Substation in southwestern Texas, and its commercial operation commenced in 2007 for interconnecting Texas Power Grid with Mexico Power Grid [69], [70]. The third VFT was successfully inaugurated among PJM power grid and NYISO power grid in 2010 [71]–[73]. The variable frequency transformer (VFT) is an engineered energy conversion device that is a mighty alternative for asynchronous grid interconnection with huge rotating inertia that provides coherent damping capability to damp out grid oscillations [74], [75].

TABLE 1. Power flow controllers used in interconnected power system networks.

PFCs	Description	Merits	Limitations	References
OLTC (on-load tap changer)	Power exchange through transmission line is regulated by controlling the magnitude of bus voltage.	Provides a variable phase-shift.	Range of power control is quite narrow.	[23], [24]
PST (phase-shifting transformer)	Power exchange through transmission line is regulated by controlling the line voltage vector.	Provides discrete phase angle shift, continually adjustable phase angle shift or a combination of duo.	• Power flow regulation is achieved in steps. • Output response is also slow.	[24], [25]
ST (sen transformer)	Regulates the voltage at a point in transmission line and independent and bidirectional control of active and reactive power transfer is also achieved.	Produces lesser losses in line with the required amount of increment in active power flow, much reduced reactive power is required.	• The control error is a function of the number of tap switches. • Response time is limited to the speed of tap switches.	[15], [26]–[28]
RPFC (rotary power flow controller)	Regulates the real and reactive power exchange by regulating the injected voltage in series with the transmission line which is not a concern of line current.	• RPFC is a deduction of two RPSTs (rotary phase-shifting transformer) thereby, enable the control of line voltage amplitude and phase angle by varying rotor angle of RPST. • In addition, regulates the flow of reactive power over shunt branch.	Requires isolated and unique drive system for rotating the rotor shaft.	[17], [22], [29]
CNT (controllable network transformer)	It has emerged from LTC (load tap changer) with the inclusion of small rating ac converter that allows the control of bus voltage vector using DVQS (dual virtual quadrature sources) technique.	• Simple and economical. • Bidirectional power flow is regulated.	• Cross-coupling between real and reactive power is achieved using the DVQS technique; hence, decoupled control is implemented using decoupled closed loop controller. • Due to presence of power electronic converters, requires adequate filtering scheme.	[30]–[32]

The VFT integrates technologies of power transformer, phase-shifter, hydro generator, doubly-fed generator, and dc drive control [76], [77].

The VFT is one of the most appealing and reliable innovations in the field of the power system in this century in the context of asynchronous interconnection. Therefore, it is necessary to have a detailed review of VFT technology developed and reported in the literature so far. This paper focuses on a comprehensive study of VFT technology used in asynchronous grid interconnection. This study includes VFT constructional details, VFT installations, comparison of VFT with back-to-back HVDC link, various control schemes utilized to improve the VFT performance, various configurations of VFT systems, including VFT park for huge power exchange and BDFIM based VFT system, and detailed mathematical model of VFT system. Moreover, simulation studies are also carried out under steady-state and various fault conditions.

C. CONTRIBUTION AND PAPER ORGANIZATION
The main contributions of this paper are stated as follows:
- A quick review of various power flow controllers, FACTS controllers, and HVDC systems, including their topologies, are presented with their technical merits and limitations along with a comparative summary.
- The VFT system and its various components are discussed in detail. Moreover, the VFT installation till date is also listed for quick view.
- Salient features of the VFT system are presented, showing better reliability and resiliency over traditional back-to-back HVDC links.
- A detailed review of control schemes employed to improve the steady-state and dynamic performance of the VFT is presented. Moreover, the VFT park model for high power exchange and brushless doubly-fed induction machine (BDFIM) based VFT system is also explored.

TABLE 2. Comparative analysis of FACTS controllers with their merits and limitations.

FACTS Contr.	Description	Merits	Limitations	References
SVC (static var compensator)	It is a variable impedance device in which the current through the reactor is regulated using back-to-back connected thyristor valves.	• Improves transient stability. • Damp out power oscillations. • Fast response. • Limits system losses by reactive power control.	• Injects the current harmonics. • Requires huge energy storage elements to compensate the var requirements. • Struggles to control the active power.	[33]–[35]
TCSC (thyristor controlled series capacitor)	Series connected type and incorporates variable impedance in transmission line.	• Increases real power transfer. • Suppressing of power oscillations. • Suppressing of sub-synchronous resonance. • Regulates power flow.	• It affects the impedance of the transmission line so there are chances of resonance problems. • Injection of harmonics.	[35]
SSSC (static synchronous series compensator)	Series connected type voltage source converter that injects voltage with adjustable magnitude and phase shift at the line frequency.	• Immunity against classical sub-synchronous and other network resonances. • Better operating characteristics. • Qualified of exchanging both real and reactive power.	Uncontrolled real power exchange.	[36], [37]
STATCOM (static synchronous compensator)	Shunt connected type voltage source converter-based device which acts as a controlled reactive power source.	• Allows instantaneous control of reactive power along with active power if provided with dc energy source. • Improves transient stability.	• Large capital investment. • Need of self-commutating power semiconductor switches.	[38], [39]
UPFC (unified power flow controller)	It is combination of STATCOM and SSSC coupled through a common dc link.	• Most powerful for control of power transfer in the transmission line. • Controls voltage magnitude. • Provides independent control of reactive var compensation.	• High cost. • Bulky.	[40], [41]
IPFC (interline power flow controller)	Series connected type which comprises of two or more SSSC coupled via dc-link.	• Provides control of real and reactive power with enhancement of bus voltage. • Regulates the flow of power across multiple lines in a network. • No need of any additional equipment for improving bus voltage level.	Creating IPFC model by managing its operational issues is an important challenge in determining the effective capabilities of the device.	[42]–[44]

• The steady-state mathematical model and simulation model in PSCAD/EMTDC of the VFT based system is developed. Moreover, the performance under steady-state and different fault conditions such as LG, LL, LLG, and LLLG are evaluated.

The remaining paper is organized as follows. In section II, the complete VFT system and its various components are discussed. In section III, salient features of the VFT system are presented. In section IV, control strategies and associated control algorithms utilized in the VFT systems are presented. In section V, the VFT configuration for high power exchange is presented. In section VI, a brushless doubly-fed induction machine (BDFIM) based VFT system, and

various configurations are reported. In section VII, detailed steady-state mathematical modeling of the VFT based system is developed. In section VIII, simulation studies is carried out under steady-state and different fault scenarios. Finally, the paper is concluded in section IX.

II. VFT SYSTEM AND ITS COMPONENTS

The VFT is essentially a continuously variable phase-shifting transformer that can operate at the controllable phase angle [78]. The essential component of the VFT is a doubly-fed induction machine (DFIM) which works as a rotating transformer, comprising of three-phase balanced windings on the stator and the rotor [79]. One power system

TABLE 3. Summary of different HVDC topologies used for asynchronous interconnection.

| HVDC Topo.	Description	Merits	Limitations	References
CSC-HVDC (current source converter type HVDC)	This topology employs thyristors and is also called as LCC (line commutated converter).	• High Power rating. • High voltage rating. • Long distance.	• Not able to sustain the power to the passive networks without the local power production. • Requires filtering scheme.	[49]–[51]
VSC-HVDC (voltage source converter type HVDC)	This topology employs IGBTs or GTOs and is also called FCC (force commutated converter).	• Used for moderate power and small length of power transmission. • Can supply power to the weak and passive networks without local power generation.	• Appreciable power loss than CSC topology. • Huge capital cost is required.	[49], [52]–[54]
MMC-HVDC (modular multilevel converter type HVDC)	It is an advanced type of MLI with a modular structure that works on medium and high-voltage applications.	• Excellent harmonic performance. • Less switching losses. • Reducing the values of the reactive components of the filter. • Reliability can be improved by increasing the number of SMs (sub-modules).	• Operation of MMC in ac drive during low frequency operation. • For the error-free operation of MMC, the capacitor voltage of the SMs (sub-modules) must be strictly constant.	[55]–[59]
HVDC light	It is an IGBT based VSC that includes converters, ac and dc switch-yards, filters and cooling systems.	• Compact structure. • Capability to quickly control both real and reactive power independently, in order to keep the voltage and frequency stable.	• Requires tuning of large number of PI controllers especially when the system parameters for the rectifier and inverter stations are different. • Particularly suitable for medium to small-scale power transmission applications.	[60], [61]
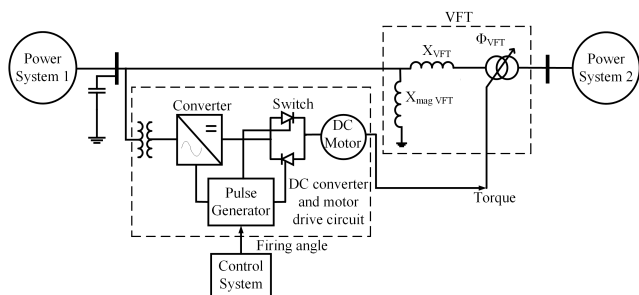
FIGURE 1. General configuration of VFT system.

is connected to the rotor while the other power system is connected to the stator of the VFT system. The various components of the VFT system are shown in Fig. 1. The VFT rotatory system consists of a rotating transformer to exchange the power between two asynchronous power systems and a drive motor to apply control torque on the rotating transformer to regulate the power flow. It also has a collector system that conducts current between the three-phase rotor winding and its stationary buswork [80].

The external DC motor provides the controlling torque. Regulation of speed and torque applied to the rotor results in a stable power exchange. When the grids' operating frequencies are the same, the rotor of VFT tries to orient in a position depending on the variance in phase angle between the two power grids. In this case, power transferred is ideally

zero. To initiate the power transfer, the rotor of VFT is allowed to rotate. Assuming applied torque in one way, power transfers from the grid have a higher phase angle to the grid having a smaller phase angle. If the applied torque is reversed, the direction of power exchange is also reversed. The net power exchange is a function of magnitude as well as the direction of torque applied to the rotor [81]. Even at idle position (when the normal operating speed of VFT is zero), the drive motor is meant to produce torque consistently. When the operating frequencies of both grids are unequal, the rotor of VFT rotates continually. Hence, the rotational speed is a function of variance in frequencies of the two grids [82]. Therefore, load flow is retained. The VFT is considered for continuous power exchange control even if there are floating frequencies on both grids. Irrespective of the power exchange, the rotor is implicitly oriented to follow the variance in phase angle set by two of the asynchronous systems. Unlike other power electronic topologies, VFT does not generate harmonics and avoids intolerable interactions with adjacent generators or other equipment on the grid [72].

III. SALIENT FEATURES OF VFT SYSTEM

The classical back-to-back HVDC link finds its practical feasibility for establishing an asynchronous interconnection between the two power systems. However, it causes serious concerns that may threaten the stability of the power

TABLE 4. Comparison of VFT with HVDC systems for an asynchronous interconnection [source:GE].

Parameter	VFT	HVDC	VSC-HVDC
High efficiency	Y	Y	-
High availability	Y	Y	Y
Low complexity	Y	-	-
Low maintenance	Y	-	-
Small space requirements	Y	N	-
Black start capability	Y	N	-
Low control interactions	Y	N	N
Low harmonic generation	Y	N	N
Low impact on adjacent generators	Y	N	N
Modular Design	Y	-	-
Easy integration with the grid	Y	N	-

[Note: Y- Yes (Best suited); N - No (Unable to perform); dash- Industry standard]

system [83]. In this context, it is essential to find an effective alternate solution. The VFT offers lead over the classical back-to-back HVDC link in the following aspects [84], [85]:

(i) Natural damping ability to suppress power oscillations because of having huge rotational inertia of the machine.

(ii) The operation is harmonics free as there are no power electronic components involved in the principal path of power exchange.

(iii) Smaller footprint because of having the large power density of a hydro generator design and no filters requirement.

(iv) Little control interface with various distinct units of the network (slower dynamics prevent any kind of control interfere with adjacent devices).

(v) High overloading capability (due to its large thermal time constant).

(vi) Isolated control of real and reactive power exchange through the VFT, and

(vii) Avoid spreading up of fault from one side to another side of the network.

Moreover, a comparison of VFT with classical HVDC and VSC-HVDC is also illustrated in the Table 4. It is revealed from the Table 4 that VFT may be a suitable alternative to back-to-back HVDC link at a broader level for realizing the asynchronous interconnection. Moreover, a description of few U.S. patents on VFT is also presented in the Table 5. A comprehensive table depicting thorough details of successful operating VFT installations so far is shown in the Table 6.

IV. CONTROL STRATEGIES USED IN VFT SYSTEM

Various control strategies are proposed in the literature to achieve smooth control over real and reactive power exchange, and reliable and secure operation of the VFT system [85]–[87]. As mentioned in Table 7, the proposed control methods can improve the dynamic response of VFT during grid disturbances and avoid the spreading of fault from one side of VFT to another side. Moreover, sufficient reactive power control and immunization against all types of asymmetrical faults are achieved.
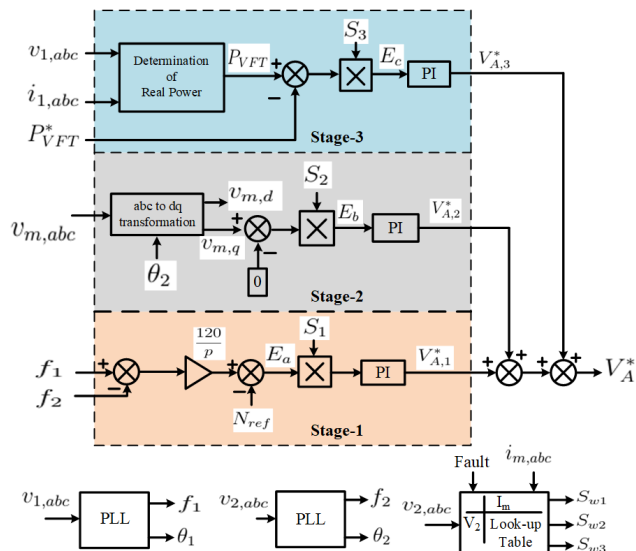

FIGURE 2. Hierarchical control scheme suggested for synchronization and control of power exchange [86].

The proposed hierarchical control scheme provides a complete control over the VFT. Moreover, a series dynamic braking resistor (SDBR) is also proposed to enhance the fault ride-through (FRT) capability of the VFT system [86]. A detailed hierarchical control including all the essential controls is represented in three stages. A practical approach to interconnect two asynchronous power systems through VFT is discussed below.

The stator of the machine is straightly tied to the PG-1 (power grid-1) having frequency f_1 and phase angle θ_1, and the rotor is directly connected to PG-2 having frequency f_2 and phase angle θ_2. To initiate the asynchronous interconnection, connect PG-1 to the stator side by closing the circuit breaker of sending end CB_{SE} meanwhile, the circuit breaker of receiving end CB_{RE} is open. During this instant, measure the frequency f_m and phase angle θ_m of the voltage induced across the rotor windings ($v_{m,abc}$) at CB_{RE} terminals. Measure the frequency f_2 and phase angle θ_2 of PG-2 voltage ($v_{2,abc}$) available on the other side of CB_{RE}. At this instant, dc motor drive is used to obtain the matching of frequency and phase angle. This controlling part is taken care in stage-1 and stage-2. Since, once the interconnection is established, power exchange is regulated in stage-3. The control block diagram explaining these three corresponding stages of the recommended hierarchical control scheme is shown in Fig. 2. The modification from one step to next step is attained using the states S_1, S_2, S_3 as mention in Fig. 2 with predetermined sequence along with SDBR protection strategy shown in Fig. 3.

A. STAGES IN HIERARCHICAL CONTROL SCHEME

1) STAGE-1: FREQUENCY COORDINATION

At first, when the stator of VFT is connected across PG-1, the rotor is idle, and CB_{RE} is open, to initiate the frequency matching step, a command $S_1 = 1$ is released. At this event,

TABLE 5. US patents granted on VFT system.

Patent No.	Title	Issues considered
US 5,952,816 (Sep 1999)	Compensation for power transfer systems using variable rotary transformer.	For asynchronous grid interconnection using variable rotary transformer, shunt and series compensating circuit are used. The shunt compensating circuit regulates the voltage by regulating the reactive current. The series compensating circuit regulates the flow of reactive power through the rotating transformer.
US 6456021 B1 (Sep 2002)	Rotating variable frequency transformer with high voltage cables.	A rotary transformer eliminates the requirement of transformer for providing the connection to a high voltage power system where either of the rotor and stator windings are high voltage cables.
US 2013/0257054 A1 (Oct 2013)	Gas turbine- Variable frequency transformer power systems and methods.	A generator coupled with gas turbine system is connected to a variable frequency transformer so that electrical power is exchanged from first grid to second grid.
US 9,450,411 B2 (Sep 2016)	Method, apparatus and system for suppressing low-frequency oscillation in power system.	A technique is suggested for damping out low-frequency oscillations in a power network by estimating the transfer function of the system where a variable frequency transformer is employed. The transfer function thus obtained for the system causes the modulation of distinctive specifications of the damping governor for the purpose of improving the network stability.

TABLE 6. Details of the VFT installation with their basic characteristics.

S. No.	Installing place	Rating of system components	Objective	Year of Operation
1	Langlois Substation, Quebec, Canada.	One 105 MVA (100 MW) and 17 kV rotary transformer; one 3000 hp DC motor along with variable-speed drive system; three sets of switched shunt capacitor each having rating of 25 MVAr; a couple of 120/17 kV traditional step-up transformer.	To recognize the tie-up between the power grids of Quebec, Canada and New York, U.S.	2003
2	Laredo Substation, U.S.	One 100 MVA and 17 kV rotary transformer; 3750 hp DC motor along with variable-speed drive system; four sets of switched shunt capacitor each having rating of 25 MVAr; a couple of 142/17.5 kV traditional step-up transformer.	Employed for establishing link between power grids of Texas, U.S. and power grids of Mexico.	2007
3	Linden Substation, U.S.	Three units are installed; each having 100 MVA and 17 kV rotary transformer; one 17 kV circuit breaker and DC motor along with variable speed drive system; single 230/17 kV step-up transformer and one 345/17 kV step-up transformer; shunt connected capacitor banks.	Employed for firming the link between PJM power grid and NY-ISO power grid.	2010

frequency of the rotor induced voltage f_m is to be changed from $f_m = f_1$ to $f_m = f_2$. In order to implement this desired frequency transform, the equivalent speed of rotor corresponding to which the rotor of VFT ought to be directed by dc motor drive is,

$$N_{ref}^* = \frac{120(f_1 - f_2)}{p} \qquad (1)$$

Thus, reference (N_{ref}^*) and actual (N_{ref}) speeds are measured against each other using comparator, and the corresponding error, E_a is generated which is further processed to the PI controller to initiate the required armature voltage ($V_{A,1}^*$) to feed dc motor. Whenever the average value of sheer speed error (E_a) falls under 1 rev/min, S_1 goes low and S_2 goes high, which introduces the next phase of the control.

2) STAGE-2: PHASE-ANGLE COORDINATION
In this stage, phase angle coordinating between ($v_{m,abc}$) and ($v_{2,abc}$) is achieved using *abc* to *dq* transformation. This *abc* to *dq* transformation is applied on the measured rotor induced voltages ($v_{m,abc}$) using phase angle (θ_2) of PG-2 voltage ($v_{2,abc}$), achieved through phase locked loop (PLL), gives the direct ($v_{m,d}$) and quadrature ($v_{m,q}$) components of the rotor induced voltages referred to PG-2 voltage phasor. By setting, $v_{m,q} = 0$, phase angle matching can be achieved. In order to implement this desired condition, a PI controller is operated through the $v_{m,q}$ to produce the required armature voltage ($V_{A,2}^*$). Whenever, the average value of sheer phase angle error, E_b falls below a pre-set margin, S_2 falls low allowing for the completion of stage-2. Once, the frequency and phase angle matching is achieved, CB_{RE} is allowed to close to

TABLE 7. Control strategies to improve the performance of VFT.

S. No.	Schemes	Description	Merits	Demerits	Ref.
1	Dynamic capability of VFT during small and large disturbances.	Small disturbance: VFT blocks power swing, Large disturbances: VFT relocate short circuit from one circuitry to another by adding impedance to stabilize a weak network.	VFT can maintain grid stability against faults for weak network interconnection and can also regulate power flow in either controlled or uncontrolled island conditions.	During the fault in the power system network, VFT demands excessive torque.	[88]
2	Spreading up of fault from one side of VFT on another side.	Fault ride-through (FRT) scheme based on series dynamic braking resistor (SDBR) is used to avoid spreading up of fault from one circuitry of VFT to another circuitry.	Alongside with regulated power exchange, VFT can successfully mitigate the propagation of fault.	Did not simulate the asymmetrical grid faults which is a stubborn concern of asynchronous grid interconnection.	[86]
3	Dissociate control of real-reactive power exchange via VFT in the asynchronous interconnection of grids.	New VFT configuration is presented with coherent partially estimated series voltage compensation measure and its associated control to implement control over reactive power exchange via VFT devoid of disturbing active power flow.	Allows the established capacitor banks to incorporate the internal reactive power demands and achieve bidirectional dissociate control of real as well as reactive power exchange.	Did not simulate the symmetrical and asymmetrical grid faults which is a major concern of asynchronous grid interconnection.	[85]
4	To immune VFT against all types of asymmetrical grid faults on both sides.	A control technique is implemented using a single series compensation converter (SCC) to immune VFT against all types of asymmetrical grid faults.	Helpful in blocking out torque and power oscillations of VFT effectively.	Big sized dc motor drive is required for rotating the VFT rotor amidst extreme fault scenarios.	[87]
5	Inability of VFT to provide sufficient reactive power compensation unlike active power.	VFT-STATCOM coordinated system is implemented to ensure the power quality with STATCOM assisting VFT with sufficient reactive power supply.	Adequate reactive power compensation is achievable, and moreover, the coordinated system also exhibits improved performance in transient conditions.	No simulations are carried out for asymmetrical faults, and proposed method is expensive.	[89]

interconnect two power grids via VFT. Eventually, S_3 goes high to initiate the power exchange controller.

3) STAGE-3: POWER EXCHANGE CONTROL

The real power transfer (P_{VFT}) from PG-1 to PG-2 is allowed to measure at the stator side of the machine and hence, is compared against the reference power (P_{VFT}^*), and the corresponding error, E_c is passed over PI controller to cause the required armature voltage ($V_{A,3}^*$) and thus, regulates the torque advanced by the dc motor drive.

B. SDBR-BASED FAULT RIDE-THROUGH CONTROL

Both the SDBR control along with error unveiling is incorporated in the hierarchical control scheme of Fig. 3. In the event of the fault at the grid, to avoid rotor acceleration, the power exchange should be controlled at its pre-fault value by forcing $S_3 = 0$ in order to have the corresponding output of the PI controller at its pre-fault value. To damp out rotor oscillations at this event, a command $S_1 = 1$ is again issued via regulating the torque of dc motor drive. At the same time, a combination of several resistors in SDBR is inserted to restrict the propagation of fault from faulted circuit to healthy one. This control is implemented with the help of a two-dimensional lookup table which is a function of VFT current and fault voltage magnitudes. The output of the lookup table defines the condition of switches S_{w1}, S_{w2}, and S_{w3} which enables the insertion of the proper combination of various resistances. Once the fault is finished, the power exchange controller is revitalized by releasing the control signals $S_1 = S_2 = 0$, $S_3 = 1$ to allow the control of power transfer.

C. DECOUPLED P-Q CONTROL

The reasons for uncontrolled reactive power flow through the VFT are (i) variations of the magnitude of the grid voltages from their nominal values, (ii) change in active power flow (magnitude and direction). The reactive power exchange through the VFT can be governed by utilizing the series voltage method of compensation. Hence, a VFT configuration is suggested that incorporates the series voltage method of compensation into the traditional VFT system to obtain complete control for reactive power exchange as shown in Fig. 4 [85].

The traditional thyristor-based dc motor drive is being replaced by IGBT based dc motor drive in the proposed configuration. This dc drive includes a shunt inverter following with dc chopper hence, allowing for a common dc-link line. The series inverter is also linked over the identical dc-link line. For the given scheme, the shunt inverter retains the voltage of the dc-link line at a fixed value
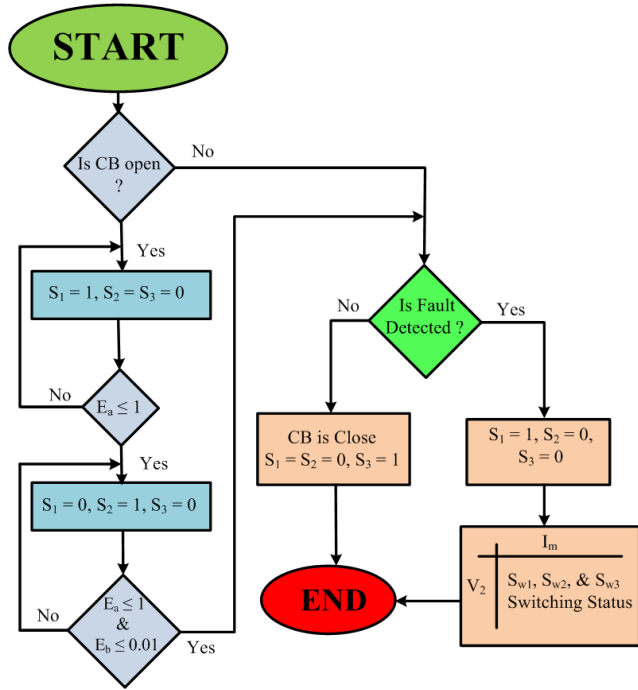
FIGURE 3. Flow diagram suggested for hierarchical control scheme and SDBR control [86].
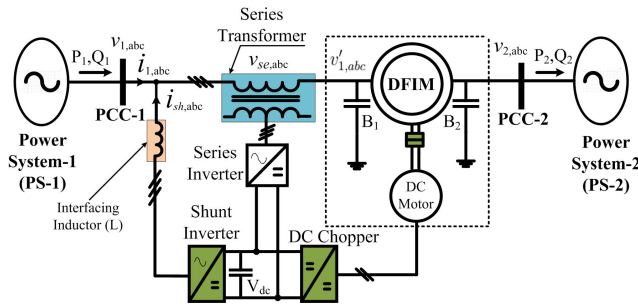

FIGURE 4. VFT configuration for independent control of real-reactive power exchange [85].

under the complete range of operation. The dc chopper is used to control the torque of dc motor by maintaining the armature voltage. The literature illustrates that the series inverter along with the series transformer provides a controllable voltage source placed in series with the stator side of the VFT.

Consequently, the effectual voltage of the grid observed on the stator side of VFT is the grid voltage available at PCC-1 plus voltage forced by the series voltage method of compensation. As far as sizing of various components is concerned, the series inverter and series transformer ratings, i.e., series voltage compensation scheme, must be ≤0.1 p.u. subjected to the condition of variation of ±5 percent in voltage magnitude of the two power grids. However, the power capacity of the dc chopper is intact. The rating of the shunt inverter is designed to handle the currents of the series inverter and dc chopper. Thus, the whole control part of the proposed scheme is completed into the following three-stages [85].
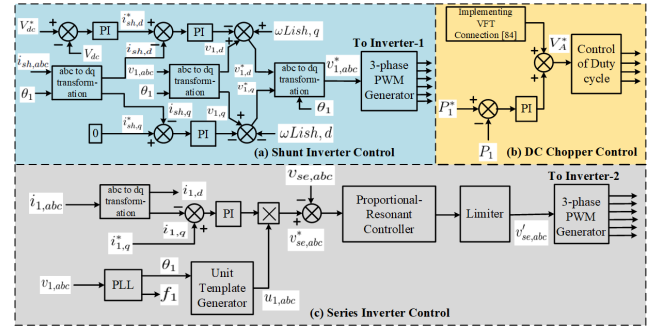

FIGURE 5. Control scheme of the proposed for independent control of real-reactive power exchange [85].

1) STAGE-1: CONTROL OF SHUNT INVERTER
The shunt inverter is used to precisely maintain the dc-link voltage at its mentioned value independent of the direction of power transfer. The equation in the synchronous reference frame of the voltage equity over the coupling inductor (L) along with an internal resistance (R) is given by [85],

$$v^*_{sh,d} = -\left(Ri_{sh,d} + L\frac{di_{sh,d}}{dt}\right) + \omega Li_{sh,q} + v_{1,d}$$

$$v^*_{sh,q} = -\left(Ri_{sh,q} + L\frac{di_{sh,q}}{dt}\right) - \omega Li_{sh,d} + v_{1,q} \qquad (2)$$

Therefore, the real and reactive powers carried by the shunt inverter is,

$$P = \frac{3}{2}v_{1,d}i_{sh,d}$$

$$Q = \frac{3}{2}v_{1,d}i_{sh,q} \qquad (3)$$

From the above equation, it is shown that $i_{sh,d}$ is used to regulate the real power and so the dc-link voltage.

2) STAGE-2: CONTROL OF DC CHOPPER
The dc chopper is used to regulate the armature voltage applied across the dc motor (V_A) to control the rotor speed of VFT. The reference value of the voltage applied across armature (V^*_A) can be produced using the control scheme discussed in [86] that enables the power exchange between the two asynchronous grids using VFT. The duty cycle control block is used to produce the duty cycle for the dc-dc converter.

3) STAGE-3: CONTROL OF SERIES INVERTER
The reactive power produced by PG-1 is a straightforward function of reactive part of stator current ($i_{1,q}$) produced. This $i_{1,q}$ becomes zero only when there is no transfer of reactive power and this situation appears when $v_{1,abc}$ and $v_{2,abc}$ have their theoretical values and $P_1 = P_2 \cong 0$. However, when $i_{1,q}$ has its non-zero value, it demonstrates reactive power transfer via VFT. Although, it can be regulated by controlling the series injected voltages ($v_{se,abc}$), which at the same time modifies the effectual grid voltage observed by VFT ($v'_{1,abc}$) using the below expression,
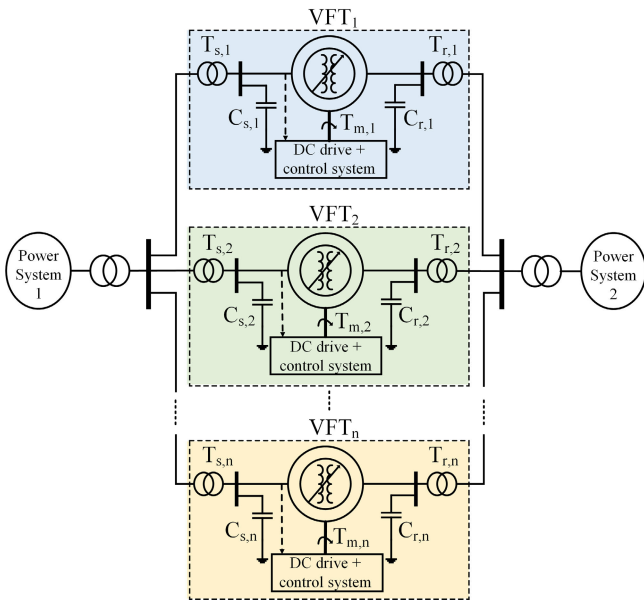
$$v'_{1,abc} = v_{1,abc} + v_{se,abc} \qquad (4)$$

FIGURE 6. Simplified VFT park model for high power transmission.

The Unit template generator can be used to produce 3-phase per-unit voltages ($u_{1,abc}$) which is having the same phase with $v_{1,abc}$. Hence, the reference value of series injected voltages ($v^*_{se,abc}$) is produced using the below expression,

$$v^*_{se,abc} = |v_{se,abc}| \times u_{1,abc} \qquad (5)$$

The controllers like proportional-resonant (PR) are required against error between the reference ($v^*_{se,abc}$) and absolute ($v_{se,abc}$) series injected voltages. This PR controllers in this particular application resonate at the fundamental frequency of PG-1 (ω_1) achieved from the PLL, and thus follows $v^*_{se,abc}$. Similarly, mutual reactive power exchange can be attained by framing the suitable per-unit value to $i^*_{1,q}$. This instantaneous restraint on the exchange of reactive current via the VFT is determined by using the following relation,

$$i^*_{1,q} \leq \sqrt{i^2_{1,rated} - (i^*_{1,d})^2}$$
$$|v^*_{se,abc}| \leq |v_{se,abc,rated}| \qquad (6)$$

It seems quite interesting to consider the regulation of effective grid voltage observed by the VFT on the stator side is equally good, contrary to the voltage of the power system connected on the rotor side.

V. VFT CONFIGURATION FOR HIGH POWER EXCHANGE
To enhance the power rating of VFT, a technique called VFT park is proposed [90]. The VFT park enables the installation of various units of VFTs operating in parallel. In the VFT park model, each VFT unit is acquired with a wound rotor induction machine (WRIM), coupling transformers, and capacitor banks [91]. Fig. 6 shows the schematic arrangement of the VFT park model.

Various techniques have developed in the recent past for evaluating the stability of VFT. Sequential continuation

scheme and limit cycle are the most commonly used. However, these methods demand the calculations of the stable operating point. The Limit cycle method determines the stable operating point of the VFT park. However, how system solutions differ by a particular parameter is determined using a continuation scheme. A continuation scheme can be established using a sequential continuation. Determination of stability and instability regions requires the sequential continuation scheme depending on the limit cycle method and Floquet theory. The calculation of the stable operating point via the limit cycle method enables effective stability studies. The stable operating point of a 300 MW VFT park is calculated via the limit cycle method under different operating conditions [92]. The simulation results demonstrate that link the rotor side of the VFT to the grid exhibits minor frequency deviations.

VI. BDFIM-BASED VFT SYSTEM
Back-to-back HVDC systems with series compensation and VFT are the two alternatives to control the power exchange in a weak interconnection [93]. However, simulations observed during steady-state and fault conditions suggest that VFT is a greater contender to control the power exchange as a bidirectional asynchronous link between the two power grids. The requirement of less reactive power, faster initial response under fault conditions, and coherent damping along with reduced generations of harmonics are the attractive features of VFT.

The VFT is a DFIM-based system that has certain limitations, such as the presence of slip rings and brushes in the rotor circuit, which results in the increment of maintenance cost and abated life span [94]. To take care, the drawbacks imposed by DFIM, BDFIM is proposed [95]. Unlike VFT, there are no slip rings and brushes, which consequently results in lowering the losses and maintenance cost [96]. The stator of the BDFIM includes a pair of three-phase windings having a different number of pole pairs [97]. One of them is placed across the grid, hence named as power winding, since it carries a major portion of the power. The second one is linked via a bidirectional converter to the grid, and it is called the control winding since it carries only a minor portion of machine power. The rotor of the BDFIM includes specially designed enclosed loops. In BDFIM, the real and the reactive power of the power winding can be controlled by governing the magnitude, frequency, and phase sequence of the applied voltage of the control winding [98]. Various configurations of BDFIM have been reported in literature [99]. Brushless duplex stator cascaded doubly-fed induction generator, Brushless doubly-fed induction generator with enclosed cage rotor, and Brushless doubly-fed induction generator with reluctance rotor. Brushless duplex stator cascaded doubly-fed induction generator requires two separate wound rotor induction machines, which consequently increases its size, complexity in speed control, and hence, cost [100].

The BDFIM with an enclosed cage rotor offers reliability and zero maintenance operation, making it suitable for

bulk power transmission. A BDFIM with an enclosed cage rotor offers alternatives against DFIM in various applications such as; adjustable speed drive for big size induction machines [101], wind applications [102], and non-contact power delivery systems [103]. However, it imposes increased losses, poor efficiency, and complexity in control due to complexity in rotor design. Moreover, a BDFIM, with a reluctance rotor, can counter the various drawbacks discussed above while retaining their benefits. But for weak networks, it may cause increased inverter rating [99]. Moreover, it also requires a complex rotor design. The BDFIM can become an alternative for asynchronous interconnection but requires special machine construction, which increases its complexity and as well as the size of the machine.

VII. DFIM THEORY AND OPERATION
The DFIM has a pair of three-phase windings accommodated in the stator and the rotor. Unlike conventional induction machines, the rotor circuit is not short-circuited, and the stator and rotor circuit is energized independently through brushes and slip rings arrangement, which enables the star as well as delta connection for rotor circuit [104]–[106].

The DFIM is very similar to a cage rotor type induction machine, but there is a slight difference in construction like; the rotor is larger for DFIM, which also requires routine care over unavoidable degradation of brushes and slip rings assembly. The stator includes a set of three-phase windings 120 degrees apart in space and having p pairs of poles. As soon as these three-phase windings are energized using a balanced three-phase voltage source having frequency f_1, due to which flux is induced in the stator, which rotates at a constant speed. This flux also interacts with the rotor circuit and induces an emf across rotor three-phase windings. This induced voltage, along with the externally supplied voltage having frequency f_2 through brushes, a current is induced through rotor three-phase windings. This induced current leads to an induced force in the rotor of DFIM. The angular frequency of the induced current in the rotor circuit is defined as [107]:

$$\omega_2 = \omega_1 - \omega_m \quad (7)$$

ω_1 is the angular frequency of the voltages and currents of the stator three-phase windings (rad/s), ω_2 is the angular frequency of the voltages and currents of the rotor three-phase windings (rad/s), ω_m is the angular frequency of the rotor (rad/s), f_1 is the electrical frequency of grid-connected on the stator side (Hz), and f_2 is the electrical frequency of grid-connected on the rotor side (Hz).

Under normal operating conditions (steady-state), ω_2 is the angular frequency of rotor winding voltage and current due to induction, and the externally supplied voltage across the rotor winding should also have ω_2 angular frequency. Hence, slip s is defined as [108]:

$$s = \frac{\omega_1 - \omega_m}{\omega_1} = \frac{\omega_2}{\omega_1} \quad (8)$$
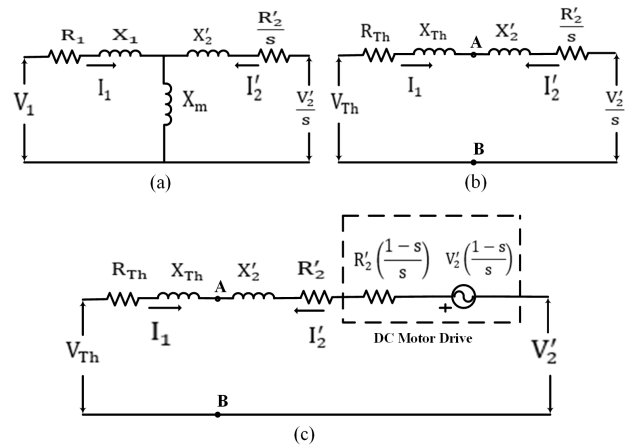

FIGURE 7. Equivalent circuit of DFIM. (a) Steady-state. (b) Thevenin's equivalent. (c) Thevenin's equivalent circuit of VFT based system.

From above expressions:

$$\omega_2 = s\omega_1 \quad (9)$$

Equivalent relation between frequencies is:

$$f_2 = sf_1 \quad (10)$$

If applied frequencies of both sides are identical ($f_1 = f_2$), in such a case, slip s becomes unity and rotor does not move and hence, DFIM appears as a non-rotating type transformer [109]. Moreover, the capacity to alter the offset location of the rotor coil with the stator coil is present due to the DC motor drive. This enables the adjustment in impedance of the transformer. When the applied frequencies of the two sides are unequal, there exist slip s and the rotor rotates at a speed that is a direct function of the difference between the stator and rotor side frequency.

A. ANALYSIS FOR POWER FLOW CONTROL
For calculating active and reactive power transfer via VFT, a steady-state equivalent circuit of VFT based system referred to the stator side is shown in Fig. 7. The terms V, I, R, X, Z, and s represent the voltage, current, resistance, reactance, impedance, and slip, respectively. While subscripts *1* and *2* denote the stator and rotor side values, respectively, and superscript $'$ denotes the quantities of rotor side when referred to stator side. It seems quite interesting to further simplify the circuit of Fig. 7 (a) by Thevenin's equivalent circuit at points AB [110], [111]. The equation for Thevenin's Voltage (V_{Th}) is expressed as:

$$V_{Th} = \left[\frac{jX_m}{R_1 + j(X_1 + X_m)} \right] V_1 \quad (11)$$

The equation for Thevenin's impedance (Z_{Th}) is expressed as:

$$Z_{Th} = \frac{jX_m(R_1 + jX_1)}{R_1 + j(X_1 + X_m)} \quad (12)$$

Further simpifying above equations yields:

$$Z_{Th} = \frac{R_1 X_m^2}{R_1^2 + (X_1 + X_m)^2} + j \left[\frac{X_m \left[R_1^2 + X_1^2 + X_1 X_m \right]}{R_1^2 + (X_1 + X_m)^2} \right] \quad (13)$$

where, the equations for R_{Th} and X_{Th} is:

$$R_{Th} = \frac{R_1 X_m^2}{R_1^2 + (X_1 + X_m)^2} \quad (14)$$

$$X_{Th} = \frac{X_m \left[R_1^2 + X_1^2 + X_1 X_m \right]}{R_1^2 + (X_1 + X_m)^2} \quad (15)$$

The current equation at sending end as derived from equivalent circuit of Fig. 7 (b) is:

$$|I_1| = \frac{|V_{Th}| - \left| \frac{V_2'}{s} \right|}{\sqrt{\left(R_{Th} + \frac{R_2'}{s} \right)^2 + (X_{Th} + X_2')^2}} \quad (16)$$

The current equation at receiving end as derived from equivalent circuit of Fig. 7 (b) is:

$$|I_2'| = \frac{\left| \frac{V_2'}{s} \right| - |V_{Th}|}{\sqrt{\left(R_{Th} + \frac{R_2'}{s} \right)^2 + (X_{Th} + X_2')^2}} \quad (17)$$

Now, splitting the terms of voltage source $\left(\frac{V_2'}{s} \right)$ and resistance $\left(\frac{R_2'}{s} \right)$ into following:

$$\frac{V_2'}{s} = V_2' + V_2' \left(\frac{1 - s}{s} \right) \quad (18)$$

$$\frac{R_2'}{s} = R_2' + R_2' \left(\frac{1 - s}{s} \right) \quad (19)$$

The terms $V_2' \left(\frac{1-s}{s} \right)$ and $R_2' \left(\frac{1-s}{s} \right)$ in expression (18) and (19) together demonstrates the mechanical power developed on the rotor by dc motor. Hence, the equivalent circuit of Fig. 7 (b) is further re-drawn in Fig. 7 (c) to certainly demonstrate the entire VFT based system containing the dc motor drive as well. Thus, the active and reactive power at sending end is expressed in equations (20) and (21):

$$P_1 = |V_1| |I_1| \cos \phi_1 + P_D \quad (20)$$

$$Q_1 = |V_1| |I_1| \sin \phi_1 \quad (21)$$

where, $\phi_1 = \angle V_1 - \angle I_1$

The active and reactive power obtained at the receiving end is expressed in equations (22) and (23):

$$P_2 = |V_2'| |I_2'| \cos \phi_2 \quad (22)$$

$$Q_2 = |V_2'| |I_2'| \sin \phi_2 \quad (23)$$

where, $\phi_2 = \angle V_2' - \angle I_2'$

The mechanical power received by the dc motor drive for the given system is calculated as [85]:

$$P_D = |V_2'| |I_2'| \left(\frac{1 - s}{s} \right) \cos \phi_2 - |I_2'|^2 R_2' \left(\frac{1 - s}{s} \right) \quad (24)$$

The torque produced by the dc motor drive under steady-state condition is obtained using equation (24):

$$T_D = P_D \left(\frac{p}{\omega_m} \right) \quad (25)$$

where, p is the pairs of pole of the machine

$$T_D = \frac{p}{\omega_m} \left(\frac{1 - s}{s} \right) \left[|V_2'| |I_2'| \cos \phi_2 - |I_2'|^2 R_2' \right] \quad (26)$$

Multiply equation (7) by slip s and further simplification give:

$$\frac{\omega_m}{\omega_2} = \left(\frac{1 - s}{s} \right) \quad (27)$$

Substituting equation (27) in equation (26) yields:

$$T_D = \frac{p}{\omega_2} \left[|V_2'| |I_2'| \cos \phi_2 - |I_2'|^2 R_2' \right] \quad (28)$$

Also,

$$T_D = \frac{p}{s\omega_1} \left[|V_2'| |I_2'| \cos \phi_2 - |I_2'|^2 R_2' \right] \quad (29)$$

VIII. SIMULATION STUDIES OF VFT SYSTEM

The two AC power systems (PS-1 and PS-2) having operating frequencies of 60 Hz and 50 Hz, respectively, are interconnected via the VFT to exchange the power as shown in Fig. 8. It is simulated using PSCAD/EMTDC software. Power System-1 (PS-1) and Power System-2 (PS-2) ratings are 240 MVA, 230 kV, 60 Hz, and 240 MVA, 230 kV, 50 Hz, respectively. The rating of VFT is 200 MVA, 20 kV. It is considered that the real power flows from PS-1 to PS-2. Hence, PS-1 is the sending end while PS-2 is the receiving end. The PS-1 is connected to the stator side of VFT via circuit breaker-1 and 230/20 kV transformer, while the PS-2 is tied to the rotor side of VFT via circuit breaker-2 and 230/20 kV transformer. A load of 100 MW, 230 kV is also connected across the two ends. Overall system response is assessed both under steady-state and fault conditions keeping torque constant at 0.95 pu. The duration of the simulation is 20 s.

A. STEADY-STATE SIMULATION
The simulation begins with the closing of circuit breaker-1, which energizes the stator side of the VFT at an instant of t = 0.5 s thereby, connecting PS-1. Later, the rotor side of the VFT is also energized at an instant of t = 1.0 s thereby, connecting PS-2. The simulated results of the three-phase sending end voltage and current are presented in Fig. 9 (a) and Fig. 9 (b), respectively. The simulated results of the three-phase receiving end (RE) voltage and current are presented in the Fig. 9 (c) and Fig. 9 (d), respectively. The value of steady-state active power at the sending end and receiving end are 215 MW and 200 MW, respectively, as depicted in Fig. 9 (e). The reactive power exchange for both sending end and receiving end are demonstrated in Fig. 9 (f). Finally, the variation of active power with respect to torque in the VFT is illustrated in Fig. 10.
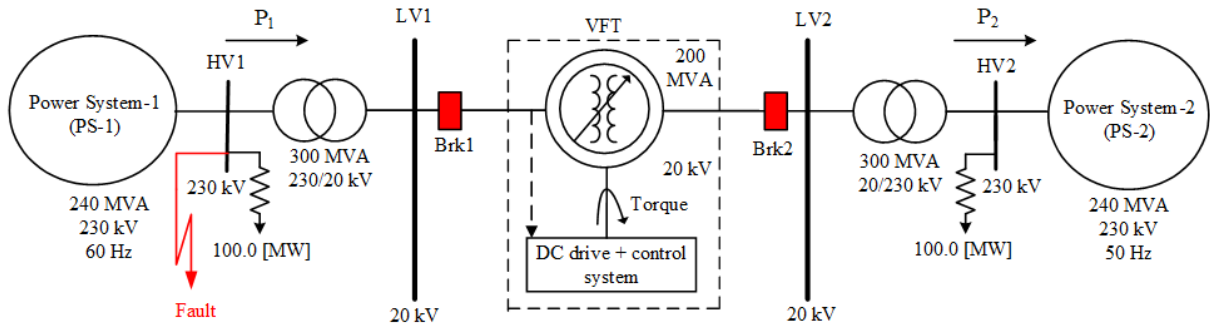
FIGURE 8. VFT configuration used for steady-state and transient simulations.

(a)

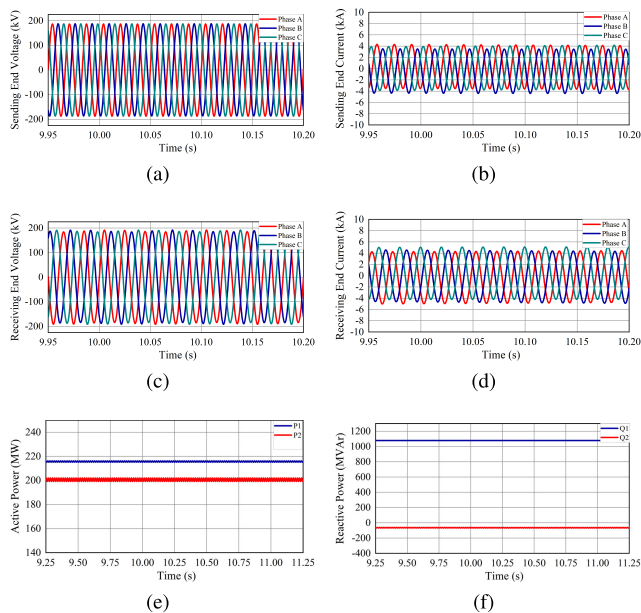
(b)

(c)

(d)

(e)

(f)

FIGURE 9. Steady-state simulation results of power transfer through VFT.
(a) Sending end voltage. (b) Sending end current. (c) Receiving end
voltage. (d) Receiving end current. (e) Active power flow at sending end
and receiving end. (f) Reactive power flow at sending end and receiving
end.

B. TRANSIENT SIMULATIONS

In this section, the performance of VFT system under different fault conditions such LG, LL, LLG, and LLLG are evaluated.

1) SINGLE-LINE TO GROUND FAULT ON SENDING END

The single-line to ground (LG) fault takes place at PS-1 (Fig. 8). The fault duration is 0.05 s (fault evolved at an instant t = 10.0 s and removed at an instant t = 10.05 s). The simulated results of the three-phase sending end voltage and current are presented in Fig. 11 (a) and Fig. 11 (b), respectively. The simulated results of the three-phase receiving end voltage and current are presented in Fig. 11 (c) and Fig. 11 (d), respectively. It is evident from Fig. 11 (b) that the sending end current of the faulty phase overshoots during the fault period and after clearance of the fault settles to its normal value. It is also illustrated from Fig. 11 (a) that the sending end voltage of the faulty phase dips during the fault period
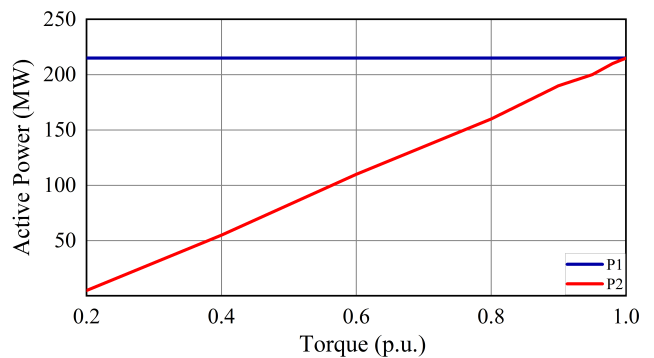

FIGURE 10. Variation of active power with respect to torque in VFT.

and after the clearance of the fault, sending end voltage of the faulty phase also regain its normal value. Moreover, the LG fault on the sending end has also an impact on the receiving end current (Fig. 11 (d)) as the receiving end current distorts during the fault, and finally settles to its normal value after the removal of the fault. However, the receiving end voltage is completely unaffected. During the LG fault on the sending end, active power experiences a dip of about 23 MW at the sending end and a comparatively smaller dip of about 20 MW at the receiving end as depicted in Fig. 11 (e). Once the fault is over, the sending end's active power is restored to its normal value of 215 MW, while the active power transferred at the receiving end is also restored to its normal value of 200 MW as depicted in Fig. 11 (e). The reactive power exchange for both sending end and receiving end are demonstrated in Fig. 11 (f). Therefore, the performance of the system is acceptable during LG fault on the sending end as the healthy side remains practically lesser affected.

2) DOUBLE-LINE FAULT ON SENDING END

The double-line (LL) fault takes place at PS-1 (Fig. 8). The fault duration is 0.05 s (fault evolved at an instant t = 10.0 s and removed at an instant t = 10.05 s). The simulated results of the three-phase sending end voltage and current are presented in Fig. 12 (a) and Fig. 12 (b), respectively. The simulated results of the three-phase receiving end voltage and current are presented in Fig. 12 (c) and Fig. 12 (d), respectively. It is apparent from Fig. 12 (b) that the sending end current of the faulty phases overshoot during the fault,
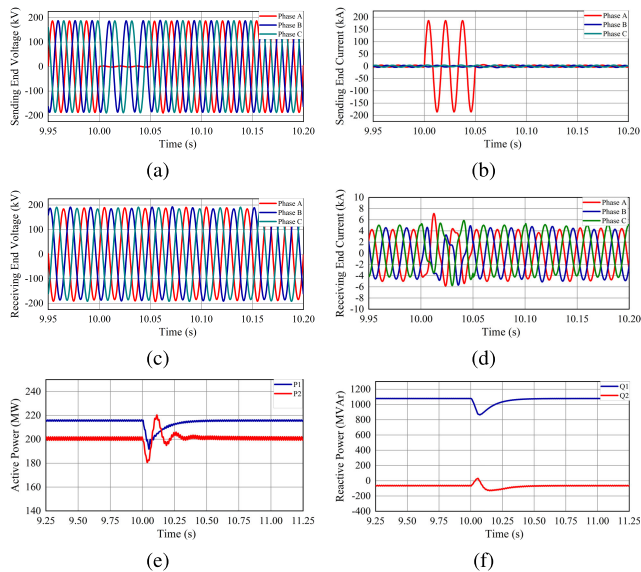
FIGURE 11. Simulation results of power transfer through VFT under LG fault condition. (a) Sending end voltage. (b) Sending end current. (c) Receiving end voltage. (d) Receiving end current. (e) Active power flow at sending end and receiving end. (f) Reactive power flow at sending end and receiving end.

FIGURE 12. Simulation results of power transfer through VFT under LL fault condition. (a) Sending end voltage. (b) Sending end current. (c) Receiving end voltage. (d) Receiving end current. (e) Active power flow at sending end and receiving end. (f) Reactive power flow at sending end and receiving end.
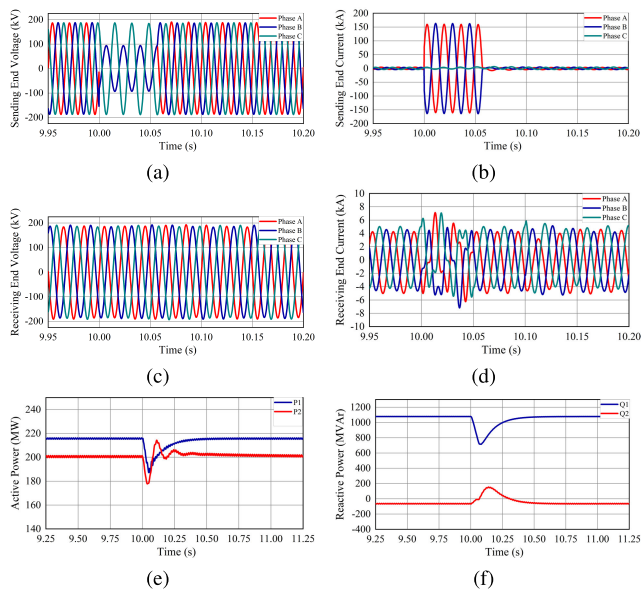
and after clearance of the fault settles to its normal values. It is also illustrated from Fig. 12 (a) that the sending end voltage of the faulty phases dip during the fault period and after the clearance of the fault, sending end voltage of the faulty phases also regain its normal values. Moreover, the LL fault on the sending end has also an impact on the receiving end current (as depicted in Fig. 12 (d)) as the receiving end current distorts during the fault, and finally settles to its normal value after the removal of the fault. However, the receiving end voltage is completely unaffected. During the LL fault on the sending end, active power experiences dip of about 29 MW
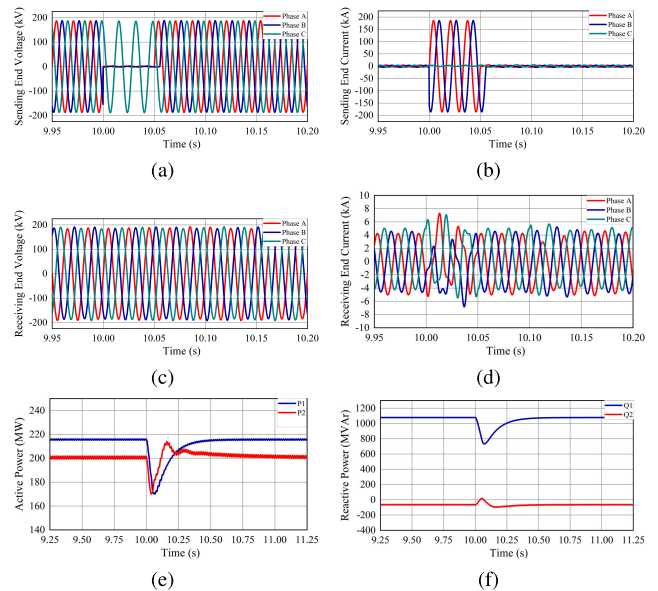

FIGURE 13. Simulation results of power transfer through VFT under LLG fault condition. (a) Sending end voltage. (b) Sending end current. (c) Receiving end voltage. (d) Receiving end current. (e) Active power flow at sending end and receiving end. (f) Reactive power flow at sending end and receiving end.

at the sending end and about 22 MW at the receiving end as depicted in Fig. 12 (e). Once the fault is over, the sending end's active power is restored to its normal value of 215 MW, while the active power transferred at the receiving end is also restored to its normal value of 200 MW as depicted in Fig. 12 (e). The reactive power exchange for both sending end and receiving end are demonstrated in Fig. 12 (f). Therefore, the performance of the system is acceptable during LL fault on the sending end.

3) DOUBLE-LINE TO GROUND FAULT ON SENDING END
The double-line to ground (LLG) fault takes place at PS-1 (Fig. 8). The fault duration is 0.05 s (fault evolved at an instant t = 10.0 s and removed at an instant t = 10.05 s). The simulated results of the three-phase sending end voltage and current are presented in Fig. 13 (a) and Fig. 13 (b), respectively. The simulated results of the three-phase receiving end voltage and current are presented in Fig. 13 (c) and Fig. 13 (d), respectively. It is evident from Fig. 13 (b) that the sending end current of the faulty phases overshoot during the fault, and after clearance of the fault settles to its normal values. It is also illustrated from Fig. 13 (a) that the sending end voltage of the faulty phases dip during the fault period and after the clearance of the fault, sending end voltage of the faulty phases also regain its normal values. Moreover, the LLG fault on the sending end has also an impact on the receiving end current (Fig. 13 (d)) as the receiving end current distorts during the fault, and finally settles to its normal value after the removal of the fault. However, the receiving end voltage is completely unaffected. During the LLG fault on the sending end, active power experiences dip of about 45 MW at the sending end and about 29 MW at the receiving end as depicted in Fig. 13 (e).
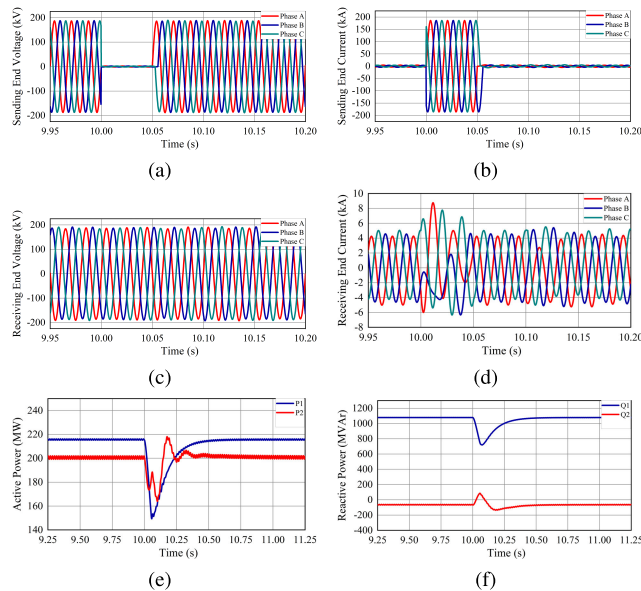
FIGURE 14. Simulation results of power transfer through VFT under LLLG fault condition. (a) Sending end voltage. (b) Sending end current. (c) Receiving end voltage. (d) Receiving end current. (e) Active power flow at sending end and receiving end. (f) Reactive power flow at sending end and receiving end.

Once the fault is over, the sending end's active power is restored to its normal value of 215 MW, while the active power transferred at the receiving end is also restored to its normal value of 200 MW as depicted in Fig. 13 (e). The reactive power exchange for both sending end and receiving end are demonstrated in Fig. 13 (f). Therefore, the performance of the system is acceptable during LLG fault on the sending end as the healthy side remains practically lesser affected.

4) TRIPLE-LINE TO GROUND FAULT ON SENDING END
The triple-line to ground (LLLG) fault takes place at PS-1 (Fig. 8). The fault duration is 0.05 s (fault evolved at an instant t = 10.0 s and removed at an instant t = 10.05 s). The simulated results of the three-phase sending end voltage and current are represented in Fig. 14 (a) and Fig. 14 (b), respectively. The simulated results of the three-phase receiving end voltage and current are represented in Fig. 14 (c) and Fig. 14 (d), respectively. It is apparent from Fig. 14 (b) that the sending end current of the faulty phases overshoot during the fault, and after clearance of the fault settles to its normal values. It is also illustrated from Fig. 14 (a) that the sending end voltage of the faulty phases dip during the fault period and after the clearance of the fault, sending end voltage of the faulty phases also regain its normal values. Moreover, the LLLG fault on the sending end has also an impact on the receiving end current (Fig. 14 (d)) as the receiving end current distorts during the fault, and finally settles to its normal value after the removal of the fault. However, the receiving end voltage is completely unaffected. During the LLLG fault on the sending end, active power experiences dip of about 65 MW at the sending end and about 35 MW at the receiving end as depicted in Fig. 14 (e). Once the fault is over, the sending end's active power is restored to its normal value of 215 MW, while the

active power transferred at the receiving end is also restored to its normal value of 200 MW as depicted in Fig. 14 (e). The reactive power exchange for both sending end and receiving end are demonstrated in Fig. 14 (f). Therefore, the performance of the system is acceptable during LLLG fault on the sending end as the healthy side remains practically lesser affected.

IX. CONCLUSION
A detailed review of asynchronous grid interconnection is carried out to evaluate a broad perspective on the different technologies proposed so far. These technologies are compared against each other with their corresponding merits and constraints. The VFT is found to be a better alternative for power transfer in a weak AC interconnection over the back-to-back HVDC link. Moreover, a comparison of the VFT with traditional back-to-back HVDC link is also carried out which suggests VFT a leading innovation over classical technology. Moreover, the VFT suppresses the power oscillations in the interconnected networks due to its inherent damping ability. Thus, it prevents cascaded tripping, the spread of effects, and grid failure of the other healthy networks. For high power exchange, the VFT park model is a better alternative where the calculation of the stable operating point via the limit cycle method offers adequate stability studies. To eliminate the periodic maintenance of slip rings and brushes, a BDFIM based VFT system is proposed, which retains all the benefits of the DFIM-based VFT system. Moreover, the performance of VFT is evaluated using mathematical modeling and simulation analysis under both steady-state and various fault conditions using PSCAD/EMTDC software. The performance of the VFT during steady-state and various fault conditions is found to be satisfactory. The simulation results prove VFT an acceptable option for asynchronous interconnection. The performance of the VFT is satisfactory as the healthy side remains less affected during fault conditions, and the fault current remains reasonably low. It is expected that this paper will work as a helpful reference for researchers and designers dealing with asynchronous interconnection.

REFERENCES
[1] R. M. Elavarasan, G. Shafiullah, S. Padmanaban, N. M. Kumar, A. Annam, A. M. Vetrichelvan, L. Mihet-Popa, and J. B. Holm-Nielsen, "A comprehensive review on renewable energy development, challenges, and policies of leading Indian states with an international perspective," *IEEE Access*, vol. 8, pp. 74432–74457, 2020.

[2] M. S. Alam, F. S. Al-Ismail, A. Salem, and M. A. Abido, "High-level penetration of renewable energy sources into grid utility: Challenges and solutions," *IEEE Access*, vol. 8, pp. 190277–190299, 2020.

[3] R. Xiong, S. M. Sharkh, H. Li, H. Bai, W. Shen, P. Bai, and X. Zhou, "IEEE access special section editorial: Advanced energy storage technologies and their applications," *IEEE Access*, vol. 8, pp. 218685–218693, 2020.

[4] M. Hossain, H. Pota, W. Issa, and M. Hossain, "Overview of AC microgrid controls with inverter-interfaced generations," *Energies*, vol. 10, no. 9, p. 1300, Aug. 2017.

[5] M. Brinkerink, B. Ó. Gallachóir, and P. Deane, "A comprehensive review on the benefits and challenges of global power grids and intercontinental interconnectors," *Renew. Sustain. Energy Rev.*, vol. 107, pp. 274–287, Jun. 2019.

[6] Imdadullah, M. Irshad, M. S. J. Asghar, and S. J. Arif, "Flexible asynchronous AC link for power system network interconnection," in *Proc. IEEE Energytech*, May 2012, pp. 1–6.

[7] N. R. Friedman, *Distributed Energy Resources Interconnection Systems: Technology Review and Research Needs*. Accessed: May 15, 2021. [Online]. Available: https://www.osti.gov/biblio/15001120

[8] D. Chen, Y. Xu, and A. Q. Huang, "Integration of DC microgrids as virtual synchronous machines into the AC grid," *IEEE Trans. Ind. Electron.*, vol. 64, no. 9, pp. 7455–7466, Sep. 2017.

[9] K. R. Padiyar and A. M. Kulkarni, *Dynamics and Control of Electric Transmission and Microgrids*. Hoboken, NJ, USA: Wiley, 2019.

[10] H. Zou, S. Mao, Y. Wang, F. Zhang, X. Chen, and L. Cheng, "A survey of energy management in interconnected multi-microgrids," *IEEE Access*, vol. 7, pp. 72158–72169, 2019.

[11] Imdadullah, H. Rahman, and M. S. J. Asghar, "A flexible asynchronous AC link for two area power system networks," *IEEE Trans. Power Del.*, vol. 34, no. 5, pp. 2039–2049, Oct. 2019.

[12] G. Chen and X. Zhou, "Digital simulation of variable frequency transformers for asynchronous interconnection in power system," in *Proc. IEEE/PES Transmiss., Distrib. Conf., Expo., Asia Pacific*, Aug. 2005, pp. 1–6.

[13] M. S. Thwala, A. F. Nnachi, K. Moloi, and A. O. Akumu, "The effect of a phase shift transformer for power flow control," in *Proc. Southern Afr. Universities Power Eng. Conf./Robot. Mechtron./Pattern Recognit. Assoc. South Afr. (SAUPEC/RobMech/PRASA)*, Jan. 2019, pp. 425–430.

[14] A. S. Siddiqui, S. Khan, S. Ahsan, M. I. Khan, and Annamalai, "Application of phase shifting transformer in Indian network," in *Proc. Int. Conf. Green Technol. (ICGT)*, Dec. 2012, pp. 186–191.

[15] J. Yuan, L. Chen, and B. Chen, "The improved sen transformer—A new effective approach to power transmission control," in *Proc. IEEE Energy Convers. Congr. Expo. (ECCE)*, Sep. 2014, pp. 724–729.

[16] K. K. Sen and M. L. Sen, "Introducing the family of 'Sen' transformers: A set of power flow controlling transformers," *IEEE Trans. Power Del.*, vol. 18, no. 1, pp. 149–157, Jan. 2003.

[17] A. O. Ba, T. Peng, and S. Lefebvre, "Rotary power-flow controller for dynamic performance evaluation—Part I: RPFC modeling," *IEEE Trans. Power Del.*, vol. 24, no. 3, pp. 1406–1416, Jul. 2009.

[18] Z. Tan, C. Zhang, and Q. Jiang, "Research on characteristics and power flow control strategy of rotary power flow controller," in *Proc. 5th Int. Youth Conf. Energy (IYCE)*, May 2015, pp. 1–8.

[19] Imdadullah, S. M. Amrr, M. S. J. Asghar, I. Ashraf, and M. Meraj, "A comprehensive review of power flow controllers in interconnected power system networks," *IEEE Access*, vol. 8, pp. 18036–18063, 2020.

[20] K. K. Sen and M. L. Sen, "Modeling of the sen transformer using an electromagnetic transients program," *HOW2POWER TODAY*, pp. 1–29, Mar. 2018.

[21] J. Yuan, L. Liu, W. Fei, L. Chen, B. Chen, and B. Chen, "Hybrid electromagnetic unified power flow controller: A novel flexible and effective approach to control power flow," *IEEE Trans. Power Del.*, vol. 33, no. 5, pp. 2061–2069, Oct. 2018.

[22] Z. Chunpeng, J. Qirong, W. Yingdong, H. Chao, C. Yan, and S. Dan, "A series voltage compensator based on thyristor-controlled transformer," in *Proc. IEEE PES Asia–Pacific Power Energy Eng. Conf. (APPEEC)*, Nov. 2015, pp. 1–5.

[23] D. Gao, Q. Lu, and J. Luo, "A new scheme for on-load tap-changer of transformers," in *Proc. Int. Conf. Power Syst. Technol.*, vol. 2, 2002, pp. 1016–1020.

[24] A. Kramer and J. Ruff, "Transformers for phase angle regulation considering the selection of on-load tap-changers," *IEEE Trans. Power Del.*, vol. 13, no. 2, pp. 518–525, Apr. 1998.

[25] J. Verboomen, D. Van Hertem, P. H. Schavemaker, W. L. Kling, and R. Belmans, "Phase shifting transformers: Principles and applications," in *Proc. Int. Conf. Future Power Syst.*, 2005, pp. 1–6.

[26] K. Sen and M. L. Sen, "Introducing the family of SEN transformers: A set of power flow controlling transformers," *IEEE Power Eng. Rev.*, vol. 22, no. 7, p. 63, Jul. 2002.

[27] K. K. Sen and M. L. Sen, "Comparison of the 'Sen' transformer with the unified power flow controller," *IEEE Trans. Power Del.*, vol. 18, no. 4, pp. 1523–1533, Oct. 2003.

[28] K. K. Sen and M. L. Sen, "Comparison of operational characteristics between a sen transformer and a phase angle regulator," in *Proc. IEEE Power Energy Soc. Gen. Meeting (PESGM)*, Jul. 2016, pp. 1–5.

[29] H. Fujita, S. Hara, K. J. Piwko, E. R. Pratico, and J. Sanchez-Gasca, "Simulator model of rotary power flow controller," in *Proc. Power Eng. Soc. Summer Meeting. Conf.*, vol. 3, 2001, pp. 1794–1797.

[30] D. Divan and J. Sastry, "Controllable network transformers," in *Proc. IEEE Power Electron. Specialists Conf.*, Jun. 2008, pp. 2340–2345.

[31] D. Das, D. M. Divan, and R. G. Harley, "Power flow control in networks using controllable network transformers," *IEEE Trans. Power Electron.*, vol. 25, no. 7, pp. 1753–1760, Jul. 2010.

[32] H. Chen, A. R. Iyer, R. G. Harley, and D. Divan, "Dynamic grid power routing using controllable network transformers (CNTs) with decoupled closed-loop controller," *IEEE Trans. Ind. Appl.*, vol. 51, no. 3, pp. 2361–2372, May/Jun. 2015.

[33] Imdadullah and M. S. J. Asghar, "Bidirectional power transmission and grid interconnections using flexible asynchronous AC transmission link," in *Proc. IEEE Int. Conf. Comput., Power Commun. Technol.*, Sep. 2019, pp. 224–229.

[34] K. Padiyar, *FACTS Controllers in Power Transmission and Distribution*. Tunbridge Wells, U.K.: Anshan, 2009.

[35] F. H. Gandoman, A. Ahmadi, A. M. Sharaf, P. Siano, J. Pou, B. Hredzak, and V. G. Agelidis, "Review of FACTS technologies and applications for power quality in smart grids with renewable energy systems," *Renew. Sustain. Energy Rev.*, vol. 82, pp. 502–514, Feb. 2018.

[36] L. Gyugyi, C. D. Schauder, and K. K. Sen, "Static synchronous series compensator: A solid-state approach to the series compensation of transmission lines," *IEEE Trans. Power Del.*, vol. 12, no. 1, pp. 406–417, Jan. 1997.

[37] A. H. Norouzi and A. M. Sharaf, "Two control schemes to enhance the dynamic performance of the STATCOM and SSSC," *IEEE Trans. Power Del.*, vol. 20, no. 1, pp. 435–442, Jan. 2005.

[38] R. M. Mathur and R. K. Varma, *Thyristor–Based FACTS Controllers for Electrical Transmission Systems*. Hoboken, NJ, USA: Wiley, 2002.

[39] P. Singh and R. Tiwari, "STATCOM model using holomorphic embedding," *IEEE Access*, vol. 7, pp. 33075–33086, 2019.

[40] L. Gyugyi, C. D. Schauder, S. L. Williams, T. R. Rietman, D. R. Torgerson, and A. Edris, "The unified power flow controller: A new approach to power transmission control," *IEEE Trans. Power Del.*, vol. 10, no. 2, pp. 1085–1097, Apr. 1995.

[41] Y. Liu, S. Yang, and F. Z. Peng, "Operation and analysis of an improved transformerless unified power flow controller," in *Proc. IEEE Appl. Power Electron. Conf. Expo. (APEC)*, Mar. 2016, pp. 959–965.

[42] T. V. Charan and A. M. Parimi, "Comparision of interline power flow controller with line reactor and SSSC in a 400kV transmission line," in *Proc. 3rd Int. Conf. Converg. Technol. (I CT)*, Apr. 2018, pp. 1–6.

[43] R. Vasquez-Arnez and F. Moreira, "Main advantages and limitations of the interline power flow controller: A steady-state analysis," *System*, vol. 1, no. 14, p. Z11, 2008.

[44] M. Ebeed, S. Kamel, and F. Jurado, "Determination of IPFC operating constraints in power flow analysis," *Int. J. Electr. Power Energy Syst.*, vol. 81, pp. 299–307, Oct. 2016.

[45] M. R. Magara, B. R. Tiwarib, R. Sharma, S. Adhikari, and S. Shresthae, "MATLAB simulation of variable frequency transformer for power transfer in-between power system networks," in *Proc. IOE Graduate Conf.*, 2019, pp. 99–105.

[46] L. Wang, S.-R. Jan, C.-N. Li, H.-W. Li, Y.-H. Huang, and Y.-T. Chen, "Analysis of an integrated offshore wind farm and seashore wave farm fed to a power grid through a variable frequency transformer," in *Proc. IEEE Power Energy Soc. Gen. Meeting*, Jul. 2011, pp. 1–7.

[47] F. I. Bakhsh, M. Irshad, and M. S. J. Asghar, "Modeling and simulation of variable frequency transformer for power transfer in-between power system networks," in *Proc. India Int. Conf. Power Electron. (IICPE)*, Jan. 2011, pp. 1–7.

[48] H. Wang and M. A. Redfern, "The advantages and disadvantages of using HVDC to interconnect AC networks," in *Proc. 45th IEEE Int. Universities Power Eng. Conf.*, Aug. 2010, pp. 1–5.

[49] C. Guo and C. Zhao, "Supply of an entirely passive AC network through a double-infeed HVDC system," *IEEE Trans. Power Electron.*, vol. 25, no. 11, pp. 2835–2841, Nov. 2010.

[50] J.-G. Lee, U. A. Khan, H.-Y. Lee, S.-W. Lim, and B.-W. Lee, "Mitigation of commutation failures in LCC–HVDC systems based on superconducting fault current limiters," *Phys. C, Supercond. Appl.*, vol. 530, pp. 160–163, Nov. 2016.

[51] A. M. Vural, "Contribution of high voltage direct current transmission systems to inter-area oscillation damping: A review," *Renew. Sustain. Energy Rev.*, vol. 57, pp. 892–915, May 2016.

[52] C. Zhao, L. Li, G. Li, and C. Guo, "A novel coordinated control strategy for improving the stability of frequency and voltage based on VSC-HVDC," in *Proc. 3rd Int. Conf. Electr. Utility Deregulation Restructuring Power Technol.*, Apr. 2008, pp. 2202–2206.

[53] S. Li, M. Zhou, Z. Liu, J. Zhang, and Y. Li, "A study on VSC-HVDC based black start compared with traditional black start," in *Proc. Int. Conf. Sustain. Power Gener. Supply*, Apr. 2009, pp. 1–6.

[54] B. Shao, S. Zhao, Y. Yang, B. Gao, and F. Blaabjerg, "Sub-synchronous oscillation characteristics and analysis of direct-drive wind farms with VSC-HVDC systems," *IEEE Trans. Sustain. Energy*, vol. 12, no. 2, pp. 1127–1140, Apr. 2021.

[55] A. R. Kumar, M. S. Bhaskar, U. Subramaniam, D. Almakhles, S. Padmanaban, and J. B.-H. Nielsen, "An improved harmonics mitigation scheme for a modular multilevel converter," *IEEE Access*, vol. 7, pp. 147244–147255, 2019.

[56] A. Elserougi, I. Abdelsalam, A. Massoud, and S. Ahmed, "Hybrid modular multilevel converter with arm-interchange concept for zero-/low-frequency operation of AC drives," *IEEE Access*, vol. 8, pp. 14756–14766, 2020.

[57] Y. Wang, A. Aksoz, T. Geury, S. B. Ozturk, O. C. Kivanc, and O. Hegazy, "A review of modular multilevel converters for stationary applications," *Appl. Sci.*, vol. 10, no. 21, p. 7719, Oct. 2020.

[58] F. Martinez-Rodrigo, D. Ramirez, A. Rey-Boué, S. Depablo, and L. C. Herrero-de Lucas, "Modular multilevel converters: Control and applications," *Energies*, vol. 10, no. 11, p. 1709, Oct. 2017.

[59] Z. Liu, K.-J. Li, J. Wang, Z. Javid, M. Wang, and K. Sun, "Research on capacitance selection for modular multi-level converter," *IEEE Trans. Power Electron.*, vol. 34, no. 9, pp. 8417–8434, Sep. 2019.

[60] D. Das, J. Pan, and S. Bala, "HVDC light for large offshore wind farm integration," in *Proc. IEEE Power Electron. Mach. Wind Appl.*, Jul. 2012, pp. 1–7.

[61] S. F. Faisal, A. R. Beig, and S. Thomas, "Time domain particle swarm optimization of PI controllers for bidirectional VSC HVDC light system," *Energies*, vol. 13, no. 4, p. 866, Feb. 2020.

[62] S. D'Arco and J. A. Suul, "Virtual synchronous machines— Classification of implementations and analysis of equivalence to droop controllers for microgrids," in *Proc. IEEE Grenoble Conf.*, Jun. 2013, pp. 1–7.

[63] L. Huang, H. Xin, and Z. Wang, "Damping low-frequency oscillations through VSC-HVDC stations operated as virtual synchronous machines," *IEEE Trans. Power Electron.*, vol. 34, no. 6, pp. 5803–5818, Jun. 2019.

[64] A. Merkhouf, P. Doyon, and S. Upadhyay, "Variable frequency transformer—Concept and electromagnetic design evaluation," *IEEE Trans. Energy Convers.*, vol. 23, no. 4, pp. 989–996, Dec. 2008.

[65] V. R. Vanajaa and N. A. Vasanthi, "Conceptual study and operational overview on variable frequency transformer used for grid interconnections," in *Proc. 3rd Int. Conf. Comput., Commun. Netw. Technol. (ICCCNT)*, Jul. 2012, pp. 1–7.

[66] R. J. Piwko, E. V. Larsen, and C. A. Wegner, "Variable frequency transformer—A new alternative for asynchronous power transfer," in *Proc. Inaugural IEEE PES Conf. Expo. Afr.*, Jul. 2005, pp. 393–398.

[67] P. Doyon, D. McLaren, M. White, Y. Li, P. Truman, E. Larsen, C. Wegner, E. Pratico, and R. Piwko, "Development of a 100 MW variable frequency transformer," presented at the Canada Power, Toronto, ON, Canada, Sep. 30, 2004.

[68] M. Dusseault, J. M. Gagnon, D. Galibois, M. Granger, D. McNabb, D. Nadeau, J. Primeau, S. Fiset, E. Larsen, G. Drobniak, and I. McIntyre, "First VFT application and commissioning," presented at the Canada Power, Toronto, ON, Canada, Sep. 30, 2004.

[69] G. Chen, X. Zhou, and R. Chen, *Variable Frequency Transformers for Large Scale Power Systems Interconnection: Theory and Applications*. Hoboken, NJ, USA: Wiley, 2018.

[70] R. Rahul, A. K. Jain, and R. Bhide, "Analysis of variable frequency transformer used in power transfer between asynchronous grids," in *Proc. IEEE Int. Conf. Power Electron., Drives Energy Syst. (PEDES)*, Dec. 2012, pp. 1–5.

[71] E. R. Pratico, C. Wegner, P. E. Marken, and J. J. Marczewski, "First multichannel VFT application—The Linden project," in *Proc. IEEE PES T D*, Apr. 2010, pp. 1–7.

[72] P. E. Marken, J. J. Marczewski, R. D'Aquila, P. Hassink, J. H. Roedel, and R. L. Bodo, "VFT—A smart transmission technology that is compatible with the existing and future grid," in *Proc. IEEE/PES Power Syst. Conf. Expo.*, Mar. 2009, pp. 1–7.

[73] J. J. Marczewski, "VFT interconnection study process with ISOs/RTOs and grid managers/operators," in *Proc. IEEE Power Eng. Soc. Gen. Meeting*, Jun. 2007, pp. 1–5.

[74] A. H. E. Din, M. A. Abdullah, and M. Ibrahim, "A MATLAB/SIMULINK model to study the performance of the VFT for the interconnection of weak and strong AC grids," in *Proc. IEEE Int. Electric Mach. Drives Conf. (IEMDC)*, May 2011, pp. 1635–1640.

[75] R. Yuan, Y. Chen, G. Chen, and Y. Sheng, "Simulation model and characteristics of variable frequency transformers used for grid interconnection," in *Proc. IEEE Power Energy Soc. Gen. Meeting*, Jul. 2009, pp. 1–5.

[76] M. Eidiani and H. Zeynal, "Flexible interconnection in energy systems via variable frequency transformer," *Majlesi J. Energy Manage.*, vol. 8, no. 3, pp. 45–53, 2019.

[77] A. Merkhouf, S. Uphadayay, and P. Doyon, "Variable frequency transformer electromagnetic design concept," in *Proc. IEEE Power Eng. Soc. Gen. Meeting*, Jun. 2007, pp. 1–6.

[78] R. J. Piwko and E. V. Larsen, "Variable frequency transformer—FACTS technology for asynchronous power transfer," in *Proc. IEEE PES Transmiss. Distrib. Conf. Expo.*, May 2005, pp. 1426–1428.

[79] A. H. E. Din, M. A. Abdullah, and M. Ibrahim, "A novel model to study the VFT performance when controlling power transfer between weak and strong AC grids using MATLAB/SIMULINK," in *Proc. IEEE Int. Energy Conf.*, Dec. 2010, pp. 189–193.

[80] A. Merkhouf, S. Upadhyay, and P. Doyon, "Variable frequency transformer—An overview," in *Proc. IEEE Power Eng. Soc. Gen. Meeting*, Jun. 2006, pp. 1–4.

[81] N. W. Miller, K. Clark, E. Larsen, R. Piwko, and G. Energy, "Variable frequency transformer provides secure inter-regional power exchange," *Energize, GE Energy*, pp. 41–44, Jun. 2006.

[82] P. Truman and N. Stranges, "A direct current torque motor for application on a variable frequency transformer," in *Proc. IEEE Power Eng. Soc. Gen. Meeting*, Jun. 2007, pp. 1–5.

[83] C. Wu, H. Zhang, Y. Hou, L. Cao, and F. Liu, "Analysis of Binjin UHVDC restart failure and relevant suggestions on secure and stable operation of power grid," *Energy Procedia*, vol. 145, pp. 452–457, Jul. 2018.

[84] Imdadullah, S. M. Amrr, A. Iqbal, and M. S. J. Asghar, "Comprehensive performance analysis of flexible asynchronous AC link under various unbalanced grid voltage conditions," *Energy Rep.*, vol. 7, pp. 750–761, Nov. 2021.

[85] B. B. Ambati and V. Khadkikar, "Variable frequency transformer configuration for decoupled active-reactive powers transfer control," *IEEE Trans. Energy Convers.*, vol. 31, no. 3, pp. 906–914, Sep. 2016.

[86] B. B. Ambati, P. Kanjiya, V. Khadkikar, M. S. E. Moursi, and J. L. Kirtley, "A hierarchical control strategy with fault ride-through capability for variable frequency transformer," *IEEE Trans. Energy Convers.*, vol. 30, no. 1, pp. 132–141, Mar. 2015.

[87] S.-Z. Chen, J. Lu, G. Zhang, and Y. Zhang, "Immunizing variable frequency transformer from dual-side asymmetrical grid faults via a single-converter-based novel control strategy," *IEEE Trans. Power Del.*, vol. 35, no. 3, pp. 1330–1338, Jun. 2020.

[88] D. Nadeau, "A 100-MW variable frequency transformer (VFT) on the Hydro-Québec TransÉnergie network—The behavior during disturbance," in *Proc. IEEE Power Eng. Soc. Gen. Meeting*, Jun. 2007, pp. 1–5.

[89] S. C S and K. Pramelakumari, "VFT-STATCOM coordinated system for improved power transfer between asynchronous grids," in *Proc. Biennial Int. Conf. Power Energy Syst., Towards Sustain. Energy (PESTSE)*, Jan. 2016, pp. 1–5.

[90] L. Contreras-Aguilar and N. Garcia, "Fast convergence to the steady-state operating point of a VFT park using the limit cycle method and a reduced order model," in *Proc. IEEE Power Energy Soc. Gen. Meeting*, Jul. 2009, pp. 1–5.

[91] L. Contreras-Aguilar and N. Garcia, "Steady-state solution of a VFT park using the limit cycle method and a reduced order model," in *Proc. IEEE Bucharest PowerTech*, Jun. 2009, pp. 1–6.

[92] L. Contreras-Aguilar and N. Garcia, "Stability analyses of a VFT park using a sequential continuation scheme and the limit cycle method," *IEEE Trans. Power Del.*, vol. 26, no. 3, pp. 1499–1507, Jul. 2011.

[93] B. Bagen, D. Jacobson, G. Lane, and H. M. Turanli, "Evaluation of the performance of back-to-back HVDC converter and variable frequency transformer for power flow control in a weak interconnection," in *Proc. IEEE Power Eng. Soc. Gen. Meeting*, Jun. 2007, pp. 1–6.

[94] P. Ledesma and J. Usaola, "Doubly fed induction generator model for transient stability analysis," *IEEE Trans. Energy Convers.*, vol. 20, no. 2, pp. 388–397, Jun. 2005.

[95] A. S. Abdel-Khalik, A. Elserougi, S. Ahmed, and A. Massoud, "Brushless doubly fed induction machine as a variable frequency transformer," in *Proc. 6th IET Int. Conf. Power Electron., Mach. Drives (PEMD)*, 2012, pp. 1–6.

[96] A. Zhang, X. Wang, W. Jia, and Y. Ma, "Indirect stator-quantities control for the brushless doubly fed induction machine," *IEEE Trans. Power Electron.*, vol. 29, no. 3, pp. 1392–1401, Mar. 2014.

[97] R. Resmi, V. Vanitha, T. Nambiar, and S. K. Kottayil, "Design and implementation of brushless doubly fed induction machine with new stator winding configuration," *Wind Eng.*, vol. 45, no. 1, pp. 11–23, Feb. 2021.

[98] S. O. Madbouly, H. F. Soliman, and A. M. Sharaf, "A new coordinated inter-coupled vector control of brushless doubly fed wind driven induction generator," *IJPEGT J.*, no. 2, pp. 1–8, 2011.

[99] M. I. Abdelkader, A. K. Abdelsalam, and A. A. Hossam, "Asynchronous grid interconnection using brushless doubly fed induction machines: Assessment on various configurations," in *Proc. 16th Int. Power Electron. Motion Control Conf. Expo.*, Sep. 2014, pp. 406–412.

[100] M. A. M. Abdulla, "New system for power transfer between two asynchronous grids using twin stator induction machine," in *Proc. IEEE Int. Electr. Mach. Drives Conf. (IEMDC)*, May 2011, pp. 1658–1663.

[101] S. Shao, E. Abdi, and R. Mcmahon, "Low-cost variable speed drive based on a brushless doubly-fed motor and a fractional unidirectional converter," *IEEE Trans. Ind. Electron.*, vol. 59, no. 1, pp. 317–325, Jan. 2012.

[102] Q. Wang, X. Chen, and Y. Ji, "Control for maximal wind energy tracing in matrix converter AC excited brushless doubly-fed wind power generation system," in *Proc. 32nd Annu. Conf. IEEE Ind. Electron. (IECON)*, Nov. 2006, pp. 718–723.

[103] A. S. Abdel-Khalik, M. I. Masoud, B. W. Williams, A. L. Mohamadein, and M. M. Ahmed, "Steady-state performance and stability analysis of mixed pole machines with electromechanical torque and rotor electric power to a shaft-mounted electrical load," *IEEE Trans. Ind. Electron.*, vol. 57, no. 1, pp. 22–34, Jan. 2010.

[104] H. Akagi and H. Sato, "Control and performance of a doubly-fed induction machine intended for a flywheel energy storage system," *IEEE Trans. Power Electron.*, vol. 17, no. 1, pp. 109–116, Jan. 2002.

[105] M. A. Poller, "Doubly-fed induction machine models for stability assessment of wind farms," in *Proc. IEEE Bologna Power Tech Conf.*, vol. 3, Jun. 2003, pp. 1–6.

[106] L. Xu and W. Cheng, "Torque and reactive power control of a doubly fed induction machine by position sensorless scheme," *IEEE Trans. Ind. Appl.*, vol. 31, no. 3, pp. 636–642, May/Jun. 1995.

[107] G. Abad, J. Lopez, M. Rodriguez, L. Marroyo, and G. Iwanski, *Doubly Fed Induction Machine: Modeling and Control for Wind Energy Generation*, vol. 85. Hoboken, NJ, USA: Wiley, 2011.

[108] H. Abu-Rub, M. Malinowski, and K. Al-Haddad, *Power Electronics for Renewable Energy Systems, Transportation and Industrial Applications*. Hoboken, NJ, USA: Wiley, 2014.

[109] B. C. Raczkowski and P. W. Sauer, "Doubly-fed induction machine analysis for power flow control," in *Proc. Electr. Insul. Conf. Electr. Manuf. Expo.*, 2005, pp. 454–459.

[110] S. Chapman, *Electric Machinery Fundamentals*. New York, NY, USA: McGraw-Hill, 2005.

[111] Imdadullah and M. S. J. Asghar, "Performance evaluation of doubly fed induction machine used in flexible asynchronous AC link for power flow control applications," in *Proc. Int. Conf. Electr., Electron. Comput. Eng. (UPCON)*, Nov. 2019, pp. 1–6.

IMDADULLAH (Senior Member, IEEE) received the bachelor's degree in electrical engineering, and the master's and Ph.D. degrees in power systems and drives from the Department of Electrical Engineering, Zakir Hussain College of Engineering and Technology, Aligarh Muslim University (AMU), Aligarh, India, in 2003, 2006, and 2020, respectively. He has about 14 years of teaching and research experience. Since December 2007, he has been working as an Assistant Professor with the Electrical Engineering Section, University Polytechnic, AMU. He has published several research articles in international journals/conference proceedings, including articles in IEEE TRANSACTIONS/journals. He holds a patent on the FASAL system, "A Concept of Flexible Asynchronous AC Link." His research interests include renewable energy, power systems, drives, instrumentation, and measurement.

JAMEL NEBHEN received the M.Sc. degree in microelectronics from the National Engineering School of Sfax, Tunisia, in 2007, and the Ph.D. degree in microelectronics from Aix-Marseille University, France, in 2012. From 2012 to 2018, he worked as a Postdoctoral Researcher with the LIRMM-Laboratory Montpellier, IM2NP-Laboratory Marseille, ISEP Paris, LE2I-Laboratory Dijon, Laboratory-Sticc Telecom Bretagne Brest, and IEMN-Laboratory Lille, France. Since 2019, he has been an Assistant Professor with Prince Sattam Bin Abdulaziz University, Alkharj, Saudi Arabia. His research interests include design of analog and RF integrated circuits, the IoT, biomedical circuit, wireless communication systems, and sensors instrumentation.

MOHD MOHSIN KHAN received the B.Tech. degree in electrical engineering from the Department of Electrical Engineering, Zakir Husain College of Engineering and Technology (ZHCET), Aligarh Muslim University (AMU), Aligarh, India, in 2018, where he is currently pursuing the M.Tech. degree in power system and drives. His research interests include power systems, and variable frequency transformer and control.

HAFIZUR RAHMAN received the B.Sc. (Engg), M.Sc. (Engg.), and Ph.D. degrees in electrical engineering from Aligarh Muslim University (AMU), Aligarh, India. From 1980 to 1985, he worked as an Electrical Engineer in India and abroad. Since 1985, he has been the Faculty of AMU, where he is currently a Professor with the Electrical Engineering Department, Z. H. College of Engineering and Technology. He has published several research articles in international journals and conferences. He was also engaged in a research project on "Simultaneous AC–DC Power Transmission" sponsored by AICTE, New Delhi, India. His research interests include HVDC, FACTS, and composite ac–dc power systems. He is a Life Member of the Indian Society for Technical Education, New Delhi.

• • •